Supplementary Information

Stress Release via Thermodynamic Regulation towards Efficient Flexible Perovskite Solar Cells

Zhiyang Xu[1,2], Runnan Yu[1,*], Tangyue Xue[3], Qiang Guo[3], Qianglong Lv[1], Chen Zhang[1], Erjun Zhou[2,*], Zhanao Tan[1,*]

[1] Beijing Advanced Innovation Center for Soft Matter Science and Engineering, College of Materials Science and Engineering, Beijing University of Chemical Technology, Beijing 100029, China

E-mail: tanzhanao@mail.buct.edu.cn (Z. Tan), yurunnan@mail.buct.edu.cn (R. Yu)

[2] College of Biological, Chemical Sciences and Engineering, Jiaxing University, Jiaxing, Zhejiang 314001, China
E-mail: zhouej@nanoctr.cn (E. Zhou)

[3] Henan Institute of Advanced Technology, Zhengzhou University, Zhengzhou 450001, China

Experimental

Materials and solvents

Isopropanol (IPA, 99.7%), *N*,*N*-dimethylformamide (DMF, 99.8%), and dimethyl sulfoxide (DMSO, 99.8%) were Acros Organics. Chlorobenzene and RbI were purchased from Sigma-Aldrich.

Flexible ITO/Polyethylene terephthalate (PET), ITO/Polyethylene naphthalate (PEN), and 2-Thiopheneethylammonium chloride (TEACl, Greatcell) were purchased from Yingkou Libra. Technology Co., LTD. [2-(3,6-dimethoxy-9H-carbazol-9-yl)ethyl]phosphonic acid (MeO-2PACz, 98.0%, TCI), Camphor (98%, Adamas-beta) and Borneol (98%, Adamas-beta) were purchased from Shanghai Titan Scientific Co., Ltd. Methylammonium bromide (MABr, Greatcell), formamidinium iodide (FAI, Greatcell), cesium iodide (CsI, 99.9%), lead(II) iodide (PbI_2, 99.99%), lead(II) bromine ($PbBr_2$, 99.999%), buckminsterfullerene (C_{60}, Nano-C, 99.5%), and bathocuproine (BCP, 99.5%) were purchased from Advanced Election Technology Co., Ltd.

Preparation of reference and camphor-modified perovskite precursor solution

The perovskite composition is $Rb_{0.05}Cs_{0.05}MA_{0.05}FA_{0.85}Pb(I_{0.95}Br_{0.05})_3$, and the initial stock perovskite solution is 1.5 M. In detail, CsI (19.5 mg), RbI (15.9 mg), MABr (8.4 mg), FAI (219.5 mg), PbI_2 (656.9 mg) and $PbBr_2$ (27.5 mg) were dissolved in 1 ml mixed solvent of DMF:DMSO (V:V = 4:1). The 1.5 M perovskite precursor solution, without filtering and dilution, was used for preparing perovskite films. Camphor-modified perovskite precursor solution was obtained by adding different concentrations (5%, 10%, 15% molar) of camphor to the perovskite precursor solution. For example, adding 11.42, 22.84, and 34.26 mg of camphor to perovskite precursor solution can obtain a perovskite precursor solution modified with 5%, 10%, and 15% camphor, respectively.

Device fabrication

After cleaning with ethanol, ITO/PET is treated with UV ozone for 15 min and can be used for spin-coating. MeO-2PACz was fabricated using mixed solvents, according to previous reports.[1] Then, the substrate covered with perovskite precursor solution was first spun at 1,000 r.p.m. for 10 s and then at 3,000 r.p.m. for 40 s. After 15 s, moving on to the second stage (3,000 r.p.m., 40 s), 150 μL chlorobenzene antisolvent was dropped on top of the spinning substrates. The substrate attached with perovskite film was subsequently annealed at 100 °C for 10 min. TEACl solution (3 mg/mL) was spin-coated on the perovskite surface at 5,000 r.p.m. for 30 s, followed by annealing at 100 °C for 5 min. Afterward, the substrate attached with perovskite film was transferred to the thermal evaporator for the sequent deposition of C_{60} (30 nm)/BCP (7 nm)/Ag (100 nm) layers, and the effective area of the device was 0.04 cm^2.

GIXRD and Photoluminescence Measurement

Grazing incident X-ray Diffraction (GIXRD) experiment was performed using a Rigaku SmartLab five-axis X-ray diffractometer equipped with Cu Kα radiation at 45 kV and 200 mA (λ = 1.54050 Å), parallel beam optics, and a secondary graphite monochromator. Before the test, the X-ray diffraction on well-recrystallized LaB6 powders was used for the subtle alignment of the instrument. GIXRD patterns were obtained by fixing the 2θ and scanning rate at 0.02° min^{-1} with the step of 0.01° by varying the instrument tilt angle (ψ), and the angle of the grazing incidence was 0.3°. The measurements were conducted using different instrument tilt angles from 0° to 50°.

In situ photoluminescence (PL) spectra were recorded on the Horiba jobin Yvon fluorolog-3 spectrofluorometer system. Through the combination of the spin-coating instrument, laser device, spectrometer, sample table, and the display screen of the spin-coating instrument, the test material is evenly coated on the glass substrate on the sample platform, the instrument parameters are set, and the laser is irradiated on the sample through the optical fiber. The spectrum of 186–1,026 nm was detected by the spectrometer, the spectral resolution reached 0.01 nm, and the time resolution reached 60 ms. The incident light at 460 nm on the film surface leads to photon excitation.

Variable temperature steady photoluminescence (PL) was measured using 520 nm as the excitation source and measured by Edinburgh FS5 spectrometer with Oxford OptistatDN liquid nitrogen temperature change test accessories. A Cu plate connected with an electric heater was used to heat the sample. Different temperatures can be realized by adjusting the electric heater input power, while we can read the temperature through the thermocouple. After reaching the set temperature and holding it for 2 minutes, we recorded the PL spectrum. Then, we slowly increased the input power and repeated the PL test when the temperature was stable at a certain point. The PL spectra were recorded at temperature steps of 10 K. The PL was normalized by the fraction of absorbed photons.

Device Characterization

The *J-V* characteristics were measured using a solar simulator (Enlitech, SS-F5-3A) with standard AM 1.5G (100 mW cm^{-2}) illumination and Keithley 2400 source, and the light intensity was calibrated using a KG-5Si diode. All tests were taken in a nitrogen glove box. The device is measured by reverse scanning (1.25 V → −0.05 V, step 0.01 V) and forward scanning (−0.05 V → 1.25 V, step 0.01 V). External quantum efficiency (EQE) data were obtained using QE-R3018, Enlitech. The transient photocurrent (TPC) and transient photovoltage (TPV) were performed with the Lst-TPCV V220804 instrumentation (Shanghai Jinzhu Tech.). The continuous light test was measured by a light simulator from Suzhou D&R Instruments Co., Ltd. A stepper tensile machine (Liaoning Shuze Solar Photovoltaic Tech. Co., LTD) was used to test the stability of the devices under different bending radii or different bending cycles. All bending test results were obtained from an average of 16 samples.

Other Characterization

The thermogravimetric analysis curves were obtained on a synchronous thermal analyzer (TGA/DSC3+). The ^{1}H NMR spectra were recorded on Bruker (AVANCE III 600 MHz). Attenuated total reflection infrared spectra (ATR-IR) were obtained on Thermo Scientific IS5. Raman spectrum was measured on Witec RAS300 Alpha300R with a 473 nm laser. X-ray photoelectron spectroscopy (XPS) was performed on a Thermo Scientific ESCALab 250 using 200 W monochromated Al Kα (1486.6 eV) radiation. Time-resolved PL spectra (TRPL) were obtained using an FLS980 spectrometer with a 475 nm EPL laser (Edinburgh Instruments Ltd.). UV–visible absorption spectra were obtained using SHIMADZU UV-2700. The scanning electron microscope (Hitachi SU8600) and the atomic force microscope (DMFASTSCAN2-SYS (Bruker) were used to characterize the film's morphology.

DFT calculations

First-principles calculations based on density functional theory (DFT) were carried out using the Vienna Ab initio Simulation Package.[2] The generalized gradient approximation of the Perdew–Burke–Ernzerhof functional was used as the exchange-correlation functional. In addition, we used the DFT-D3 method for the van der Waals correction and also dipole corrections for the slab calculations. A plane-wave cut-off energy of 400 eV was used. The energy and force convergence criteria were set to 10^{-5} eV and 0.03 eV Å^{-1}, respectively. The Brillouin zone was sampled with Γ-centred k-mesh densities of $2\pi \times 0.02$ Å^{-1} in the calculations of the energetic and electronic properties. We used a vacuum of 20 Å to separate neighboring surfaces in the z-direction. The binding energies (E_b) of different molecules (camphor and borneol) with the perovskite surface were calculated as $E_{mol/pvsk} - E_{pvsk} - E_{mol}$, where $E_{mol/pvsk}$, E_{pvsk}, and E_{mol} are the total energies of the adsorption system, the perovskite system and molecules (borneol and camphor), respectively. The electrostatic potentials (φ) of molecules were calculated using the Gaussian 09 package at the B3LYP/def2TZVP level with DFT-D3.

Supplemental Formulas

$$\boldsymbol{\sigma} = -\frac{E\,\pi}{2(1+\nu)180^{\circ}} \cdot \cot\theta_0 \frac{\partial(2\theta)}{\partial sin^2(\Psi)} \tag{1}$$

$$\boldsymbol{\varepsilon} = \frac{\sigma}{E} \tag{2}$$

Where $\boldsymbol{\sigma}$ is the stress; $\boldsymbol{E}$ and $\boldsymbol{\upsilon}$ are Young's modulus and Poisson's ratio of the thin film, respectively, and $\boldsymbol{\upsilon} \approx 0.3$; θ_0 is the diffraction peak for stress-free perovskite crystal plane (hkl), and $\boldsymbol{\theta}$ is the diffraction peak for the actual perovskite thin films; $\frac{\partial(2\theta)}{\partial sin^2(\Psi)}$ is slope of fitting; $\boldsymbol{\varepsilon}$ is strain.[3][4]

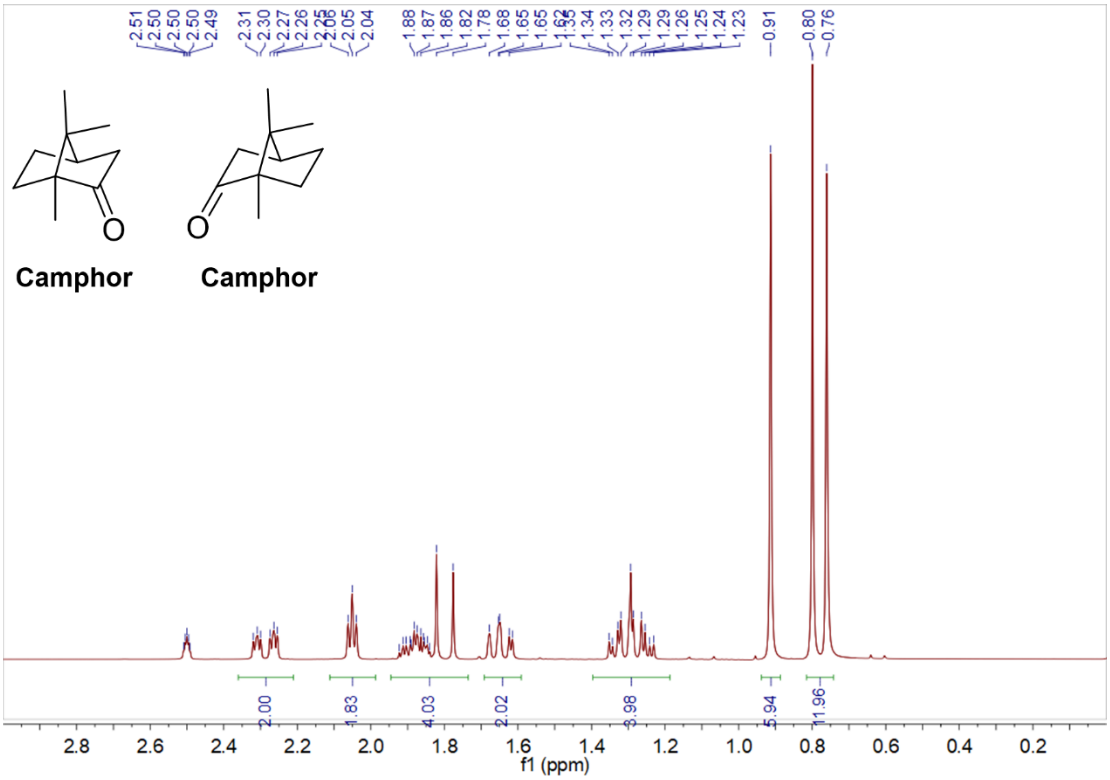

Fig. S1 ^{1}H NMR spectra of Camphor that have chiral properties in *d*-C_2D_6SO.

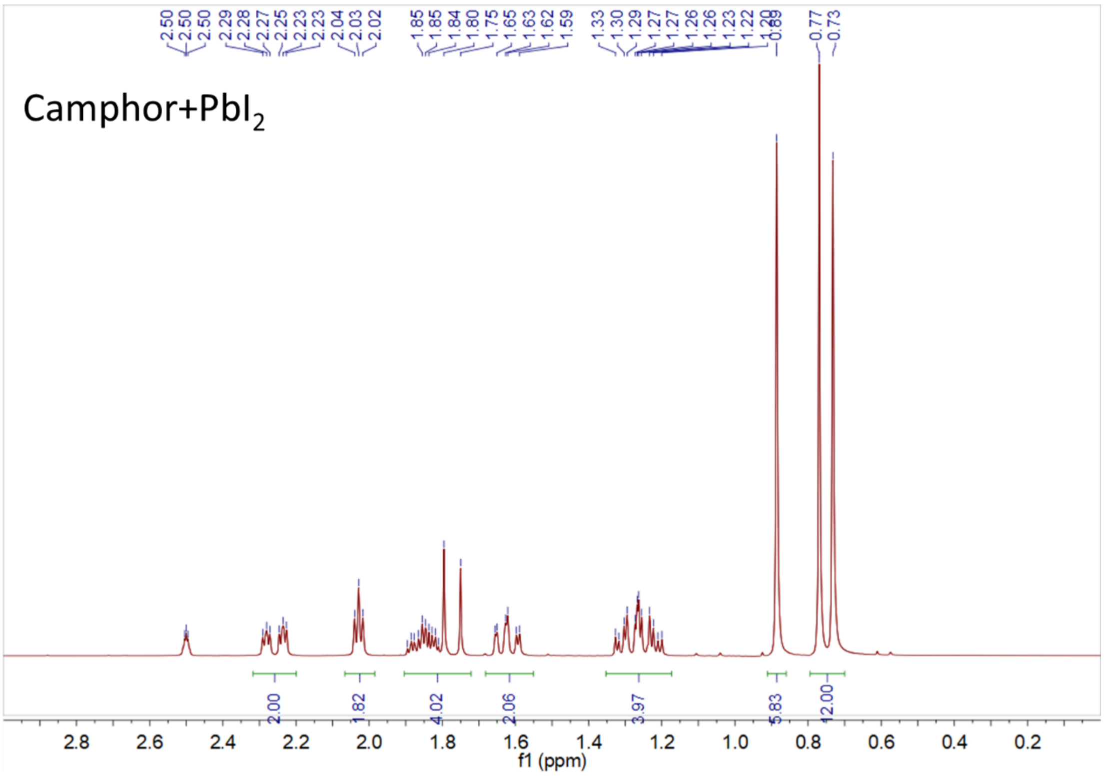

Fig. S2 ^{1}H NMR spectra of Camphor and PbI_2 in *d*-C_2D_6SO.

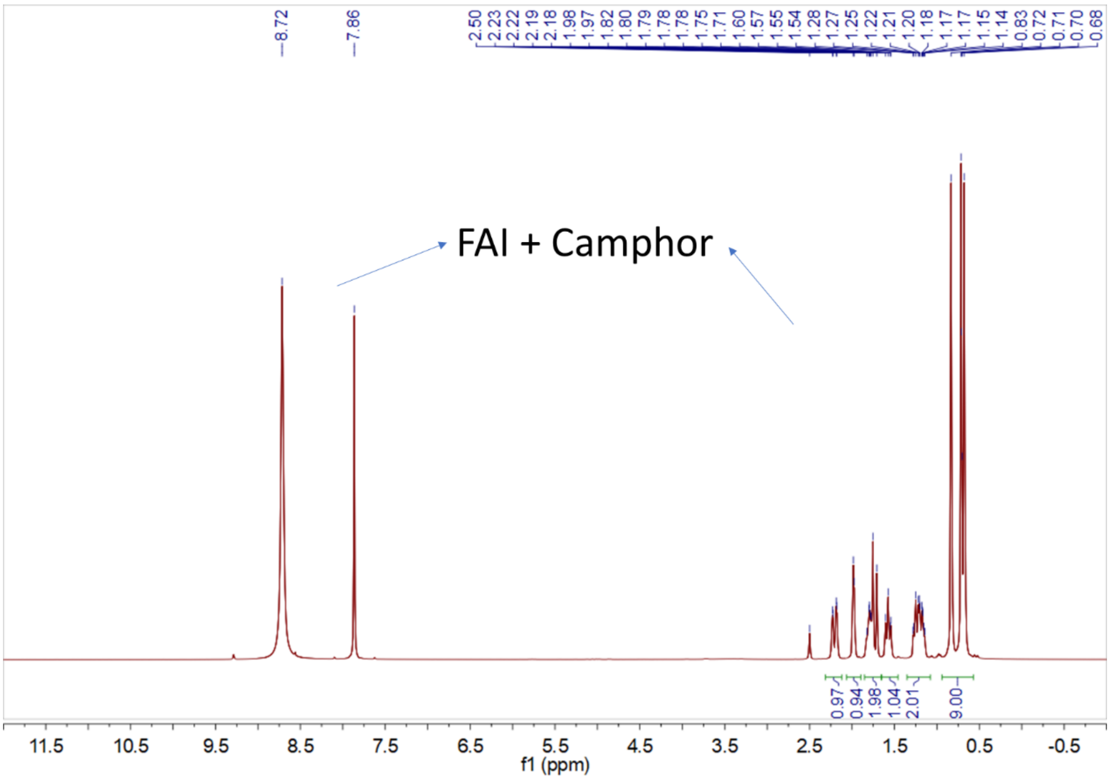

Fig. S3 ^{1}H NMR spectra of Camphor and FAI in *d*-C_2D_6SO.

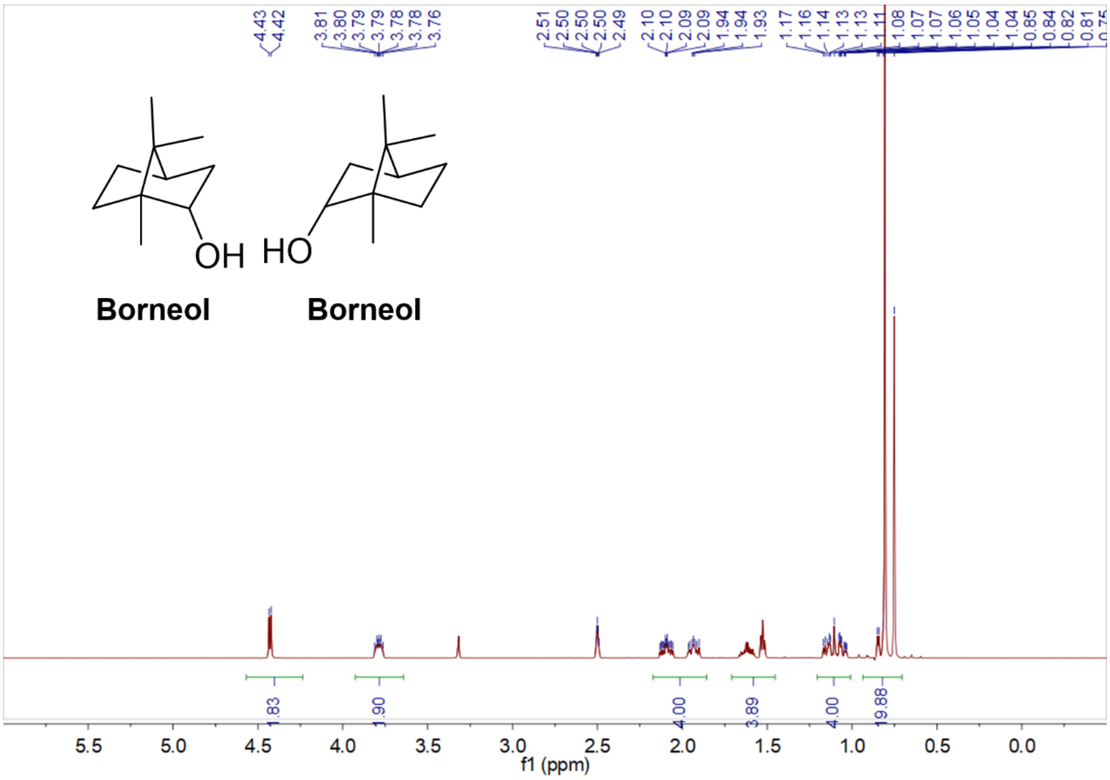

Fig. S4 ^{1}H NMR spectra of Borneol in *d*-C_2D_6SO.

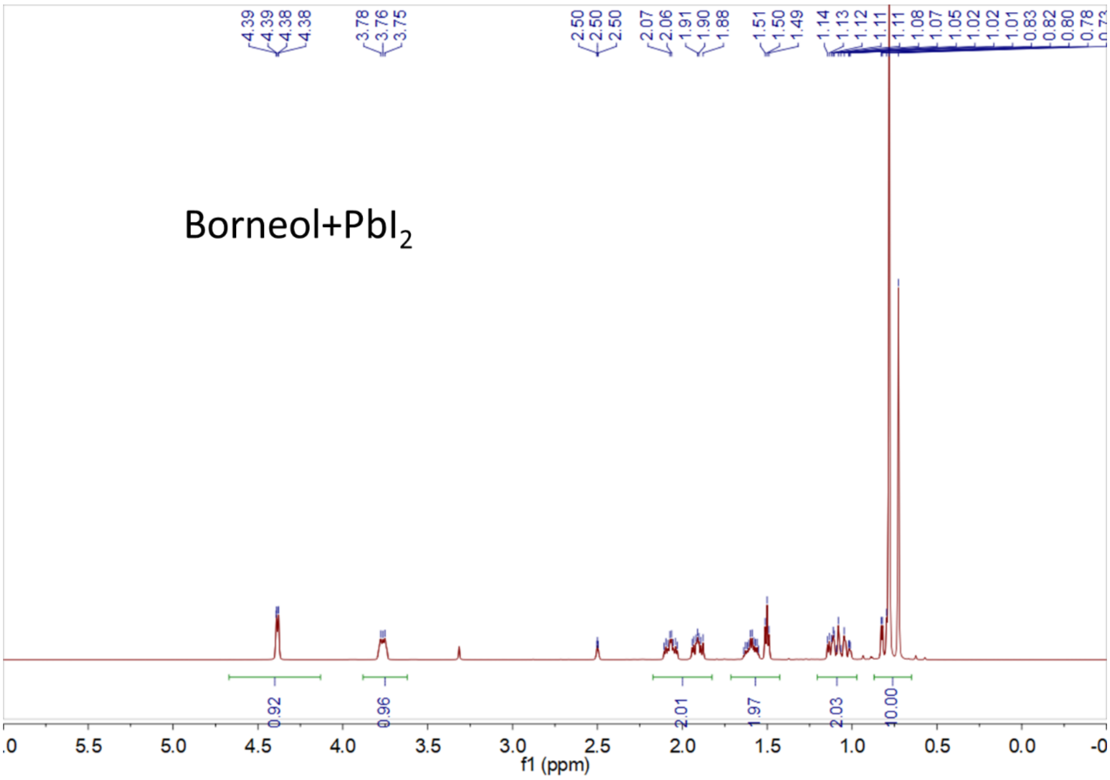

Fig. S5 ^{1}H NMR spectra of Borneol and PbI_2 in *d*-C_2D_6SO.

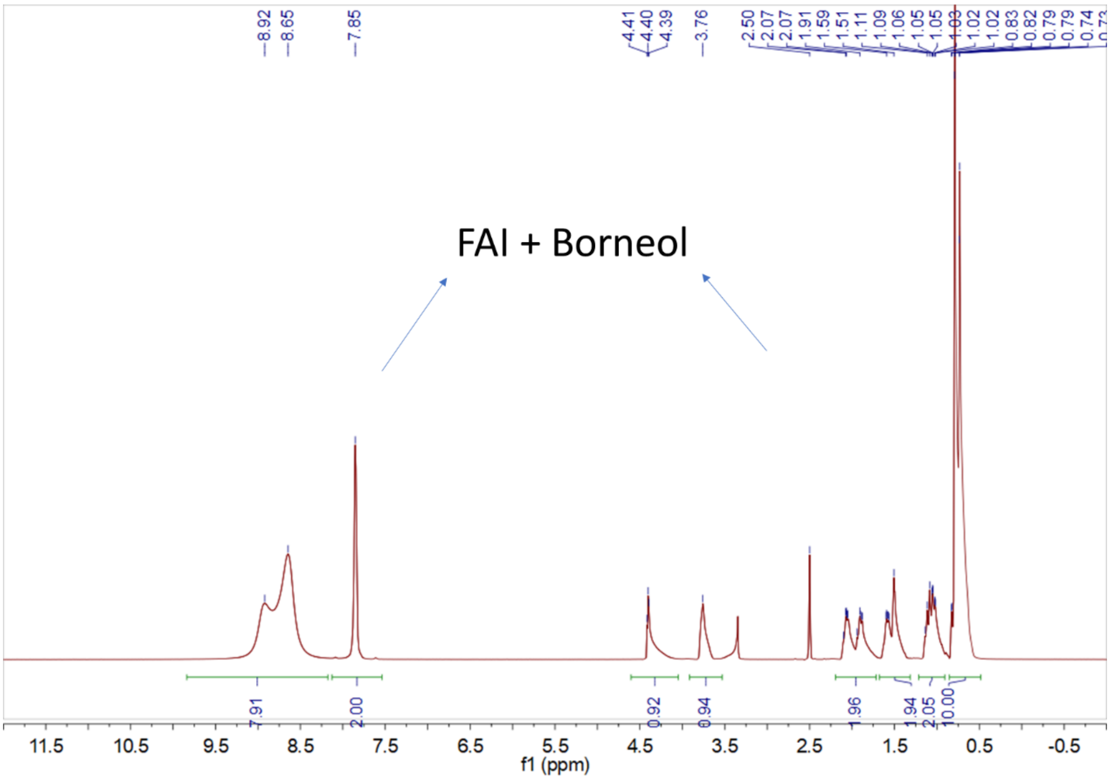

Fig. S6 ^{1}H NMR spectra of Borneol and FAI in *d*-C_2D_6SO.

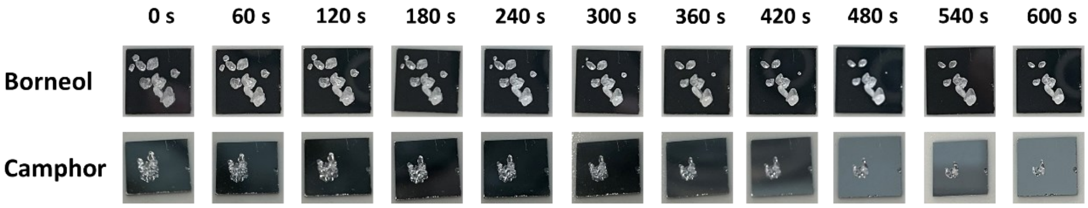

Fig. S7 Optical photographs of 20 mg camphor or borneol at different times on the 100 °C heating plate.

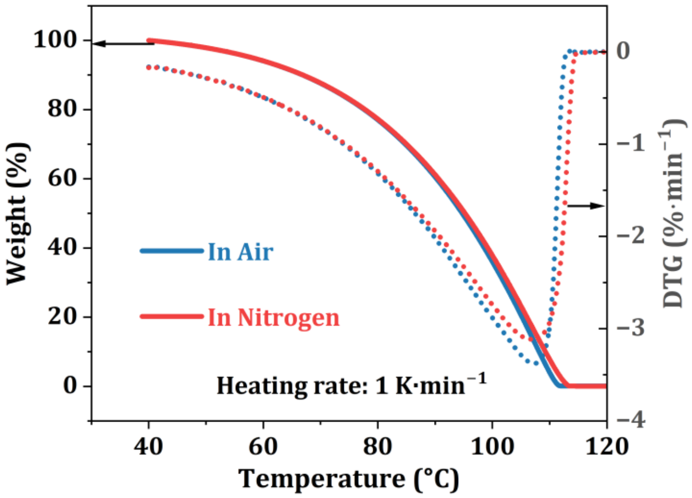

Fig. S8 TGA of camphor under the Nitrogen and dry air conditions, respectively.

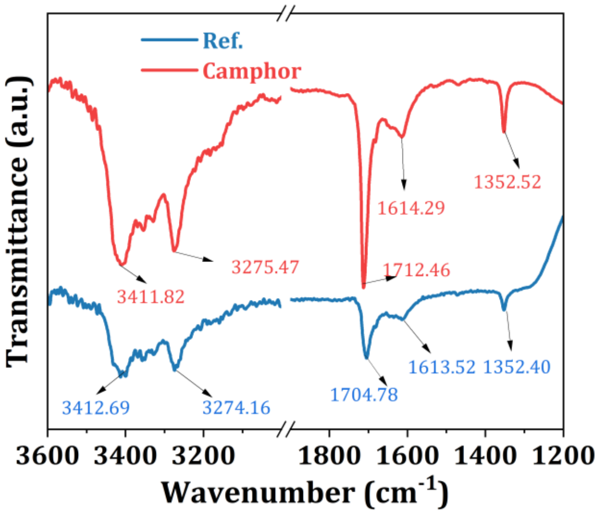

Fig. S9 IR spectra of the reference and camphor-modified perovskite films.

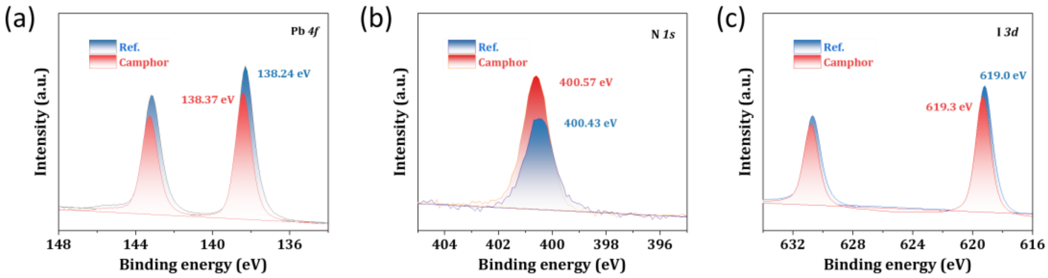

Fig. S10 High-resolution XPS spectra of *Pb 4f* (**a**), *N 1s* (**b**), and *I 3d* (**c**) for the reference and camphor-based perovskite films.

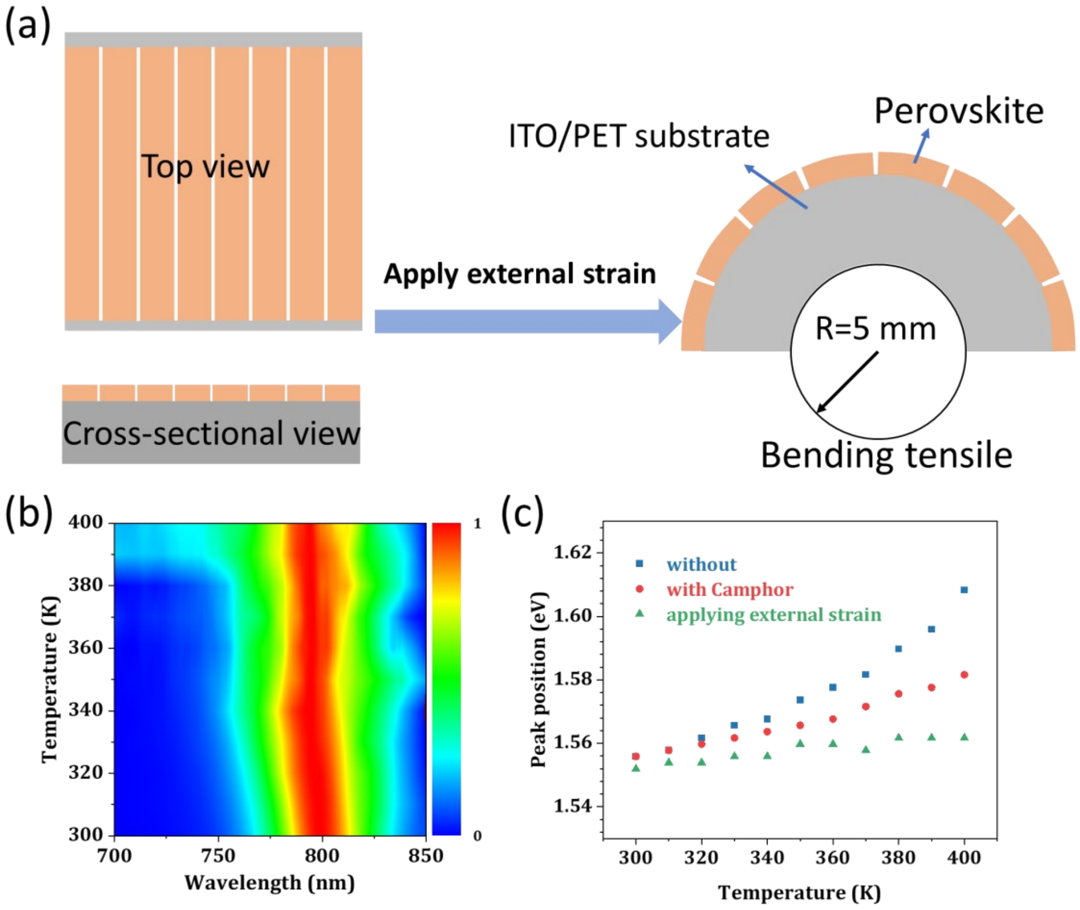

Fig. S11 (a) Schematic diagram of an additional strain applied to a perovskite film. The camphor-based perovskite film is subjected to 1000 bending cycles to execute external strain. **(b)** Normalized PL spectra versus temperature of the camphor-based perovskite film after applying external strain. **(c)** PL peak positions versus temperature for different perovskite films.

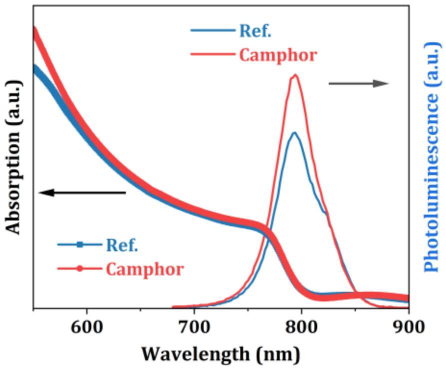

Fig. S12 UV-visible and PL spectra of the reference and camphor-based perovskite films.

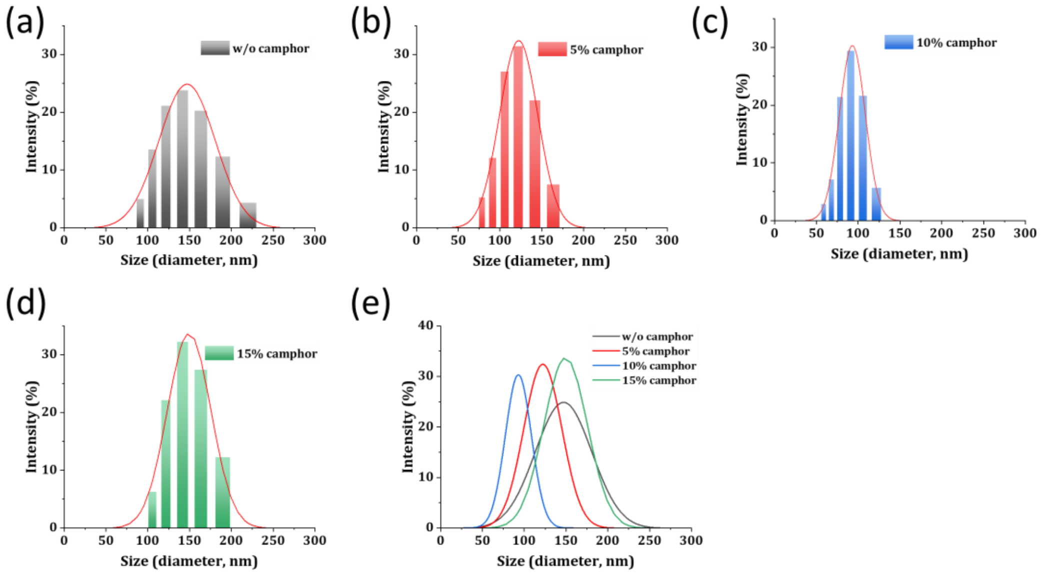

Fig. S13 (a-d) Colloid size distributions of perovskite precursor solution withdifferent concentrations of camphor. **(e)** Comparison of particle size distributions after Gauss fitting.

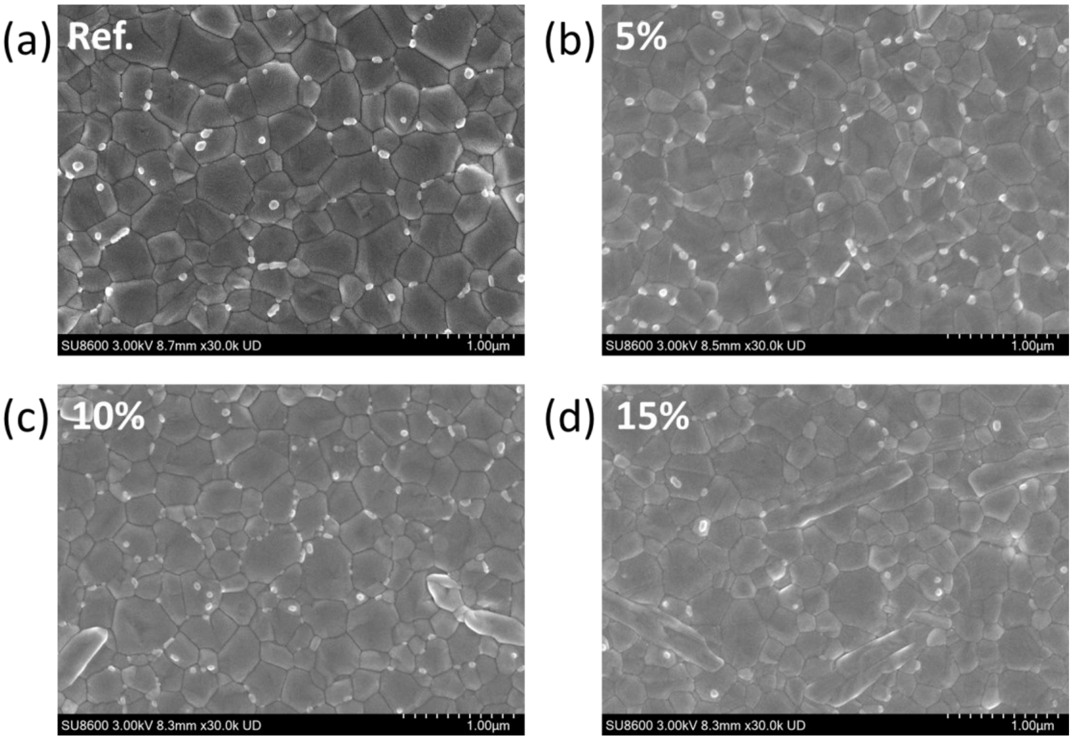

Fig. S14 SEM images of the perovskite films prepared by precursor solution with different concentrations of camphor.

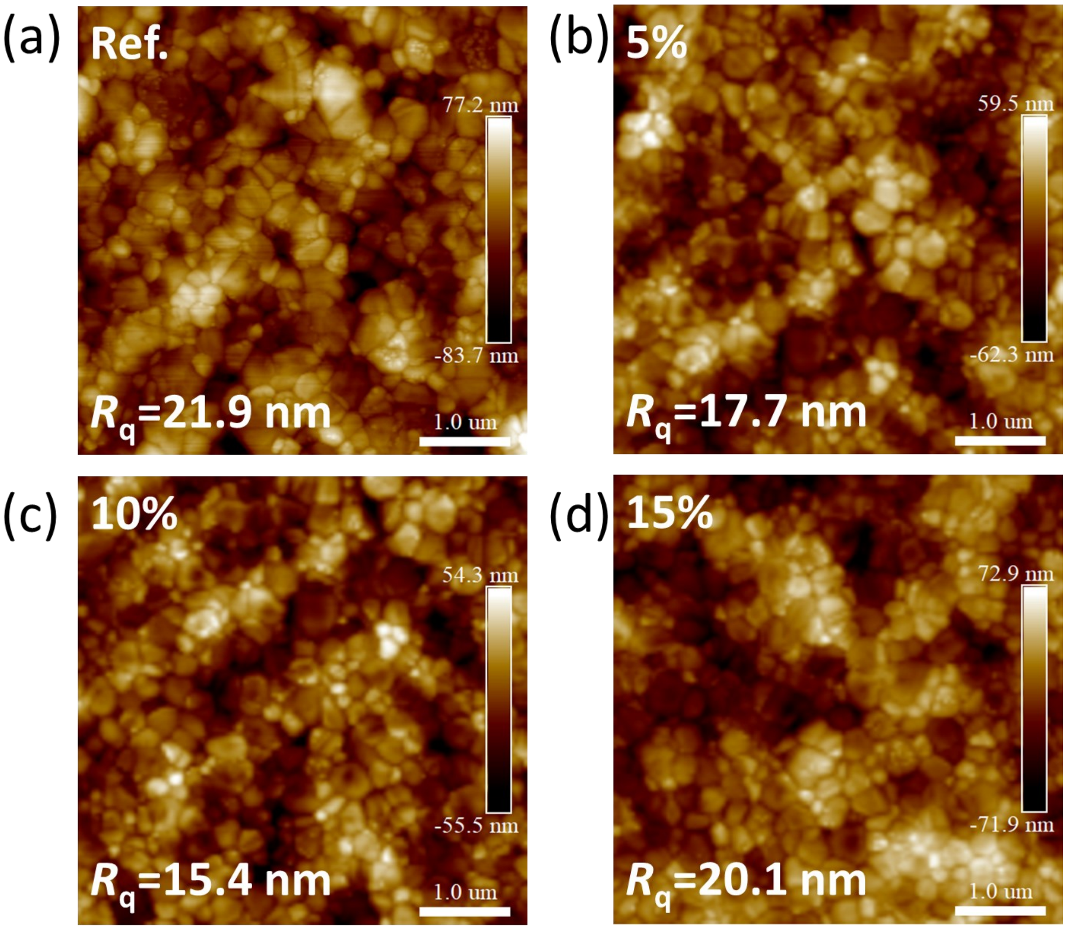

Fig. S15 AFM images of the perovskite films prepared by precursor solution with different concentrations of camphor.

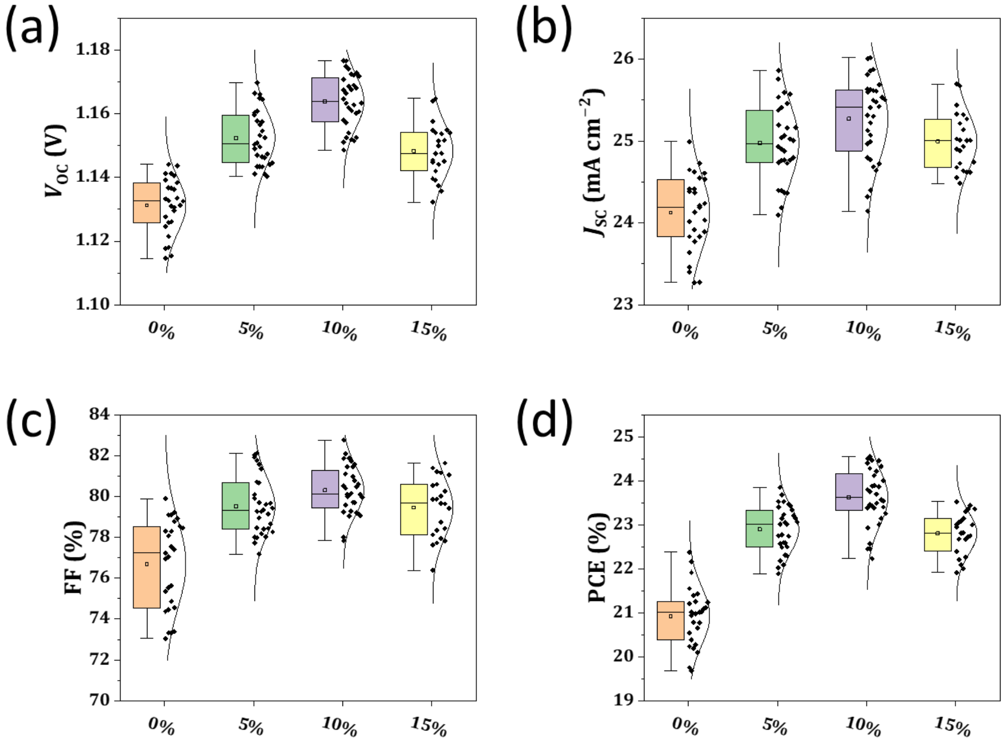

Fig. S16 The statistical distribution of photovoltaic parameters: (**a**) V_{OC}, (**b**) J_{SC}, (**c**) FF, (**d**) PCE.

PHOTOVOLTAIC AND WIND POWER SYSTEMS QUALITY TEST CENTER, IEE, CHINESE ACADEMY OF SCIENCES

Report No: PWQC-WT-P24040121-4R

Testing information:

Date：April, 01, 2024

Location：No.6 Bei-er-tiao, Zhongguancun, Haidian district, Beijing, China

Environmental conditions：(24.9±2)℃, (40.9±5)%RH

Testing items：

Measurement of photovoltaic current-voltage characteristics

Standards：

IEC 60904-1：2006 Photovoltaic (PV) devices
— Part 1：Measurement of photovoltaic current-voltage characteristics

Equipments：

Name	S/N	Expired date
Solar simulator	LE106-04	2024-10-15
Source Meter	LE177-01	2025-04-01
Reference cell	J-CH04	2025-04-06

Edited by(signatory)：

Approved by(signatory)：

Page 1 of 5

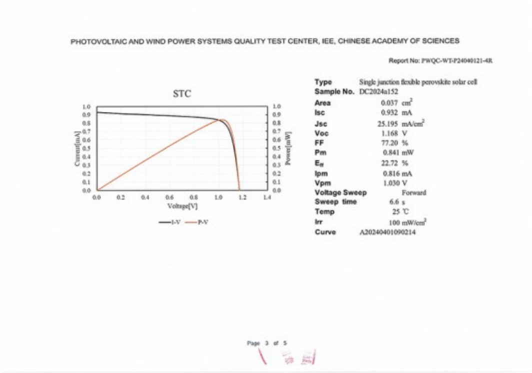

PHOTOVOLTAIC AND WIND POWER SYSTEMS QUALITY TEST CENTER, IEE, CHINESE ACADEMY OF SCIENCES

Report No: PWQC-WT-P24040121-4R

Type	Single junction flexible perovskite solar cell
Sample No.	DC2024a152
Area	0.037 cm^2
Isc	0.932 mA
Jsc	25.195 mA/cm^2
Voc	1.168 V
FF	77.20 %
Pm	0.841 mW
E$_{ff}$	22.72 %
Ipm	0.816 mA
Vpm	1.030 V
Voltage Sweep	Forward
Sweep time	6.6 s
Temp	25 ℃
Irr	100 mW/cm^2
Curve	A20240401090214

Page 3 of 5

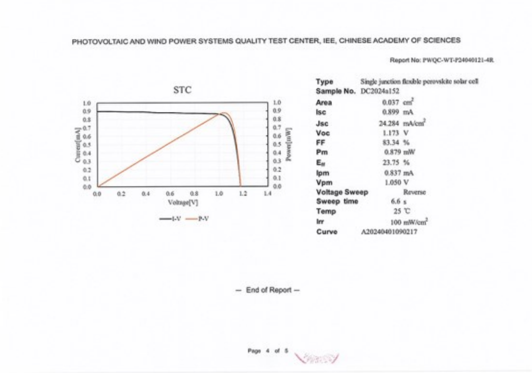

PHOTOVOLTAIC AND WIND POWER SYSTEMS QUALITY TEST CENTER, IEE, CHINESE ACADEMY OF SCIENCES

Report No: PWQC-WT-P24040121-4R

Type	Single junction flexible perovskite solar cell
Sample No.	DC2024a152
Area	0.037 cm^2
Isc	0.899 mA
Jsc	24.284 mA/cm^2
Voc	1.173 V
FF	83.34 %
Pm	0.879 mW
E$_{ff}$	23.75 %
Ipm	0.837 mA
Vpm	1.050 V
Voltage Sweep	Reverse
Sweep time	6.6 s
Temp	25 ℃
Irr	100 mW/cm^2
Curve	A20240401090217

— End of Report —

Page 4 of 5

Fig. S17 The efficiency certification report for the camphor-based f-PSCs from the IEE, Chinese Academy of Sciences, China.

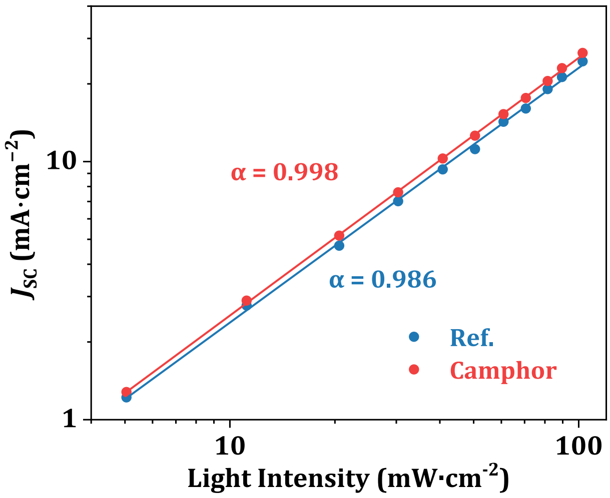

Fig. S18 J_{SC} versus light intensity of different f-PSCs.

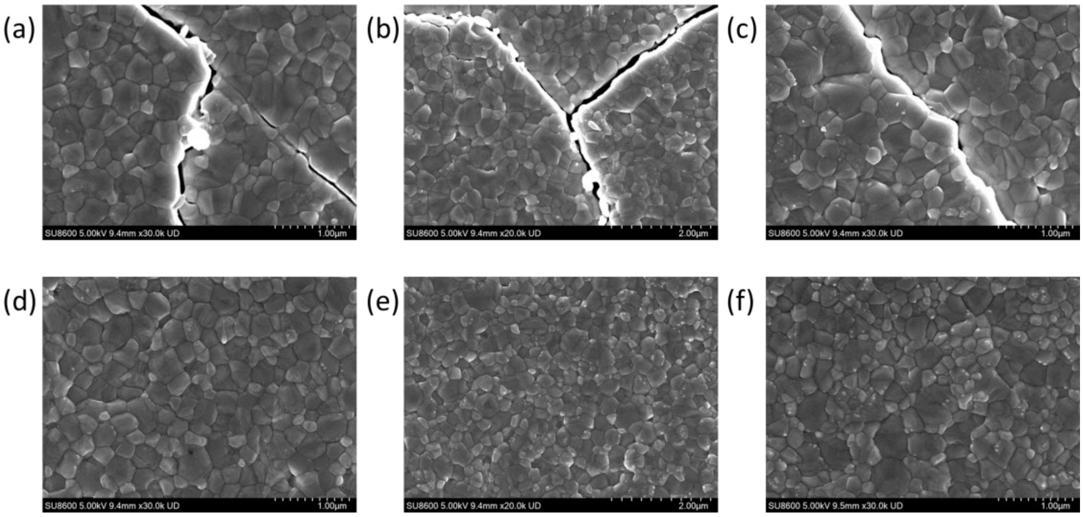

Fig. S19 SEM images of perovskite film at different positions after bending. **(a)** the left part, **(b)** the middle part, **(c)** the right part of the reference film. **(d)** the left part, **(e)** the middle part, **(f)** the right part of the camphor-based film.

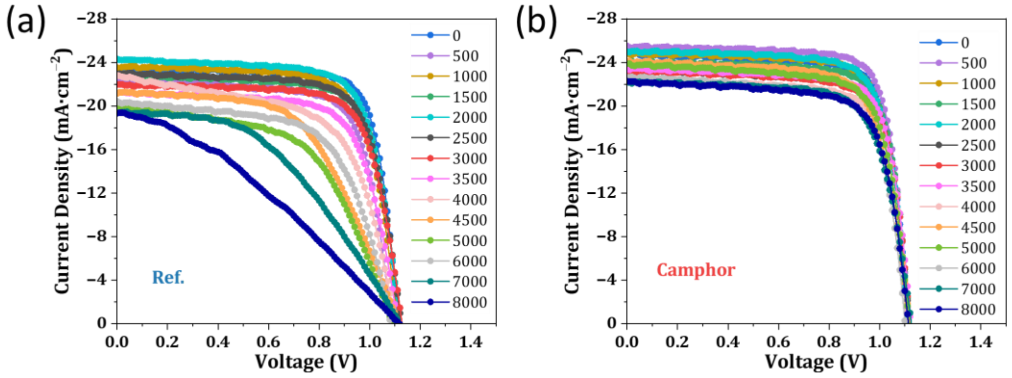

Fig. S20 *J*–*V* characteristics of (**a**)the reference and (**b**) camphor-based f-PSCs undergoing different bending cycles.

Table S1. Fitted information from Raman spectra for the reference perovskite film.

Peak Index	Peak Type	Area Intg	FWHM	Max Height	Center Grvty	Area IntgP
1	Lorentz	73273.36407	33.55973	1464.15212	126.60475	30.38798
2	Lorentz	74859.22447	52.39014	973.07898	160.83786	31.04567
3	Lorentz	92993.53413	103.03122	638.47536	227.97712	38.56635

Table S2. Fitted information from Raman spectra for the camphor-based perovskite film.

Peak Index	Peak Type	Area Intg	FWHM	Max Height	Center Grvty	Area IntgP
1	Lorentz	73273.36407	33.55973	1464.15212	126.60475	30.38798
2	Lorentz	74859.22447	52.39014	973.07898	160.83786	31.04567
3	Lorentz	92993.53413	103.03122	638.47536	227.97712	38.56635

Table S3. Fitted parameters from TRPL spectra for the reference and camphor-based perovskite films.

	τ_1 (ns)	B1	τ_2 (ns)	B2	τ_{ave} (ns)
Ref.	90.55	7.17%	792.858	92.83%	742.5025
Camphor	111.6993	7.62%	1064.899	92.38%	992.2656

Table S4. Parameters derived from EIS measurements for the different devices.

Sample	R_s (Ω)	R_{ct} (Ω)	C1-T	C1-P	R_{rec} (Ω)	C2-T	C2-P
Ref.	61.6	149.4	1.0×10^{-8}	0.80	32.2	2.5×10^{-4}	0.77
Camphor	56.8	134.8	3.4×10^{-8}	0.89	50.9	1.4×10^{-4}	0.92

Reference

[1] Liu, M.; Bi, L.; Jiang, W.; Zeng, Z.; Tsang, S. W.; Lin, F. R.; Jen, A. K., Compact Hole-Selective Self-Assembled Monolayers Enabled by Disassembling Micelles in Solution for Efficient Perovskite Solar Cells. *Adv. Mater.* **2023**, 35 (46), 2304415.

[2] Lin, R.; Xu, J.; Wei, M.; Wang, Y.; Qin, Z.; Liu, Z.; Wu, J.; Xiao, K.; Chen, B.; Park, S. M.; Chen, G.; Atapattu, H. R.; Graham, K. R.; Xu, J.; Zhu, J.; Li, L.; Zhang, C.; Sargent, E. H.; Tan, H., All-perovskite tandem solar cells with improved grain surface passivation. *Nature* **2022**, 603 (7899), 73-78.

[3] Zhu, C.; Niu, X.; Fu, Y.; Li, N.; Hu, C.; Chen, Y.; He, X.; Na, G.; Liu, P.; Zai, H.; Ge, Y.; Lu, Y.; Ke, X.; Bai, Y.; Yang, S.; Chen, P.; Li, Y.; Sui, M.; Zhang, L.; Zhou, H.; Chen, Q., Strain engineering in perovskite solar cells and its impacts on carrier dynamics. *Nat. Commun.* **2019**, 10 (1), 815.

[4] Yu, J.; Wang, M.; Lin, S., Probing the Soft and Nanoductile Mechanical Nature of Single and Polycrystalline Organic-Inorganic Hybrid Perovskites for Flexible Functional Devices. *ACS Nano* **2016**, 10 (12), 11044-11057.